Smart Structures and Systems, *Vol. 28, No. 5 (2021) 593-603*
https://doi.org/10.12989/sss.2021.28.5.593

Damage monitoring of variable cross-section region in a column-drilled shaft assembly using smart aggregates

Jie Tan [1,2], Mahadi Masud [3], Xiaoming Qin [4], Cheng Yuan [4], Qingzhao Kong*[4] and Y.L. Mo**[3]

[1] *Hubei Key Laboratory of Earthquake Early Warning, Institute of Seismology, CEA, Wuhan, China*
[2] *Wuhan Institute of Earthquake Engineering Co., Ltd., Wuhan, China*
[3] *Department of Civil and Environmental Engineering, University of Houston, TX, USA*
[4] *Disaster Mitigation for Structure, College of Civil Engineering, Tongji University, Shanghai, China*

(*Received October 16, 2020, Revised April 14, 2021, Accepted May 7, 2021*)

Abstract. Pier column, as the most critical load-bearing member of bridge, can bear multiple loads including axial forces, shear forces, bending moments, etc. The varied cross section at the column interface and bearing platform or drilled shaft leads to harmful stress concentration that can potentially compromise the structural integrity. In order to improve the ductility of bridge structure, a pier column is often designed with a variable cross-section region to dissipate energy through plastic deformation. For better understanding the health condition of pier column in its service life, it is of great significance to obtain the damage severity information in the variable cross-section region. This study utilizes an active sensing method enabled by distributed Lead Zirconate Titanate (PZT)-based Smart Aggregate (SA) sensors to monitor the damage initiation and development near the bottom of a pier column. Crack damage in variable cross-section region functions as a stress relief that attenuates propagating stress wave energy between SA pairs. Both the numerical and experimental results show that the reduction ratio of the stress wave energy is consistent with the crack development, thus validating the reliability of the investigated approach. SA-based technology can be used as a potential tool to provide early warning of damage in variable cross-section region of bridge structures.

Keywords: active sensing approach; pier column; PZT; smart aggregate; structural health monitoring; variable cross-section region

1. Introduction

Bridge plays a crucial role in urban transportation system. In a bridge structure, the pier column is an important load-bearing element that bears vertical loads (e.g., the weight of the bridge and the passing vehicles) and horizontal loads transmitted from beams (e.g., the loads induced by acceleration and braking of the vehicles, seismic loads, and wind loads). In addition to potential harsh load conditions, the stress concentration induced by steep variations in cross section at the junction of pier column and the platform or drilled shaft makes the column foundation area be more prone to occur damage. Numerous investigations of bridge-related disasters show that many bridge collapses are initiated with the pier column destruction. In order to enhance the ductility of the bridge structure, the bottom of the pier column is often designed with a variable cross-section region (Berry *et al*. 2008, Motaref *et al*. 2014), as shown in Fig. 1. In such design, overload-induced damage occurs first in the variable cross-section region and the input energy is mostly dissipated. There is great utility in monitoring the occurrence and development of cracks in bridge column variable cross-section region to gauge damage severity and provide early warnings, thereby avoiding bridge collapse and the associated undesirable consequences.

In recent years, piezoelectric sensors (Huo *et al*. 2019, Kong *et al*. 2017b, c, Karayannis *et al*. 2015) and fiber-optic sensors (Li *et al*. 2004, Pan *et al*. 2006) have facilitated the rapid innovation of structural health monitoring technology. Piezoelectric-based methods mainly include active sensing methods (Kong *et al*. 2013, Jiang *et al*. 2019, Zou *et al*. 2019), electro-mechanical impedance methods (Liang *et al*. 2016, Huynh *et al*. 2015) and passive

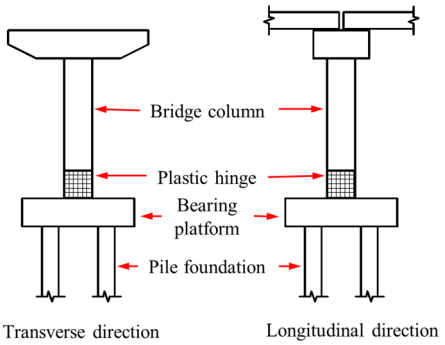

Fig. 1 Variable cross-section design at the bottom of a bridge column

*Corresponding author, Professor,
E-mail: qkong@tongji.edu.cn
**Co-corresponding author, Professor

ISSN: 1738-1584 (Print), 1738-1991 (Online)

(a) Illustration of a smart aggregate (b) A smart aggregate with a BNC connector

Fig. 2 Smart aggregate transducer

acoustic emission methods (Banjara *et al*. 2019, Li *et al*. 2016). Fiber-optic-based technologies including fiber Bragg gratings (Kuang and Cantwell 2003) and distributed fiber optic sensing (Feng *et al*. 2020) have been widely used in civil structural health monitoring. Particularly of note is piezoceramic smart aggregate (SA), which is a relatively new type of transducer consisting of a lead zirconate titanate (PZT) patch integrated within a protective marble case (Song *et al*. 2008), as shown in Fig. 2(a). Fig. 2(b) shows a fabricated SA that can be used for experiments. The SA boasts many advantages in field structural health monitoring, such as robust reliability, great durability, cost effectiveness, broadband frequency response, simplicity of implementation, and dual functions as actuator and sensor (Yan *et al*. 2009, Liu *et al*. 2013, Yao *et al*. 2015, Kong *et al*. 2017a).

The unique superiority of SAs has attracted many researchers to investigate their potential applications for health monitoring of a wide variety of civil structures. In SA-based active sensing technique, the characteristics of the stress wave signal sent from the actuator to the sensor is closely related to the propagation medium properties. Based on this phenomenon, many studies have been reported to monitor the damage severity of key structural members, including concrete pipe (Feng *et al*. 2015), concrete pile (Feng *et al*. 2016), reinforced concrete columns (Kong *et al*. 2016, Howser *et al*. 2011, Gu *et al*. 2010), steel bolts (Wang *et al*. 2017, 2020), and timber structures (Zhang *et al*. 2018a, b). These studies demonstrated that the occurrence and development of damage in the propagation medium significantly reduces the energy of the stress wave signal. Taking the initial, undamaged state of the propagation medium as the healthy baseline, the level of internal damage and the approximate health status of the component can be inferred by monitoring the loss ratio of the propagated stress wave energy. Using similar principles, piezoceramic sensors have been applied for monitoring the bond slip between different materials. Qin *et al*. (2015) analyzed the stress waves propagating between an SA in concrete and a SA installed on the steel plate to SA monitor the bond slip of steel plate concrete structure. Results showed that the process of bond slip can be monitored accurately and gauged through a damage index commonly used in active sensing approaches. Similar results have been obtained in other experiments, including the monitoring of bond slip in composite structures encased in concrete (Zeng *et al*. 2015) and in FRP reinforced concrete structures (Jiang *et al*. 2020). In addition to experimental applications, numerical simulations of piezoelectric materials have further confirmed the feasibility and effectiveness of the active sensing approach (Markovic *et al*. 2015, Quant *et al*. 2009).

While SAs are favored for their excellent performance in health monitoring, SAs have not been used to monitor damage initiation and crack development in regions with varied cross sections. In this paper, SAs are embedded in the variable cross-section region of a column-drilled shaft assembly to monitor the internal damage process of the region while undergoing monotonic bending loads. In both numerical and experimental study, it can be seen that the received sensing signal decreases with the increase of the crack dimension located in variable cross-section region. A Wavelet packet-based damage index is adopted to quantitatively evaluate the column-drilled shaft condition.

2. Active sensing approach

Piezoelectric materials can exhibit both the converse and the direct piezoelectric effects, which allow dual functionality as actuators and sensors (Hou *et al*. 2012, 2013, Nguyen *et al*. 2013). These properties enable piezoelectric materials to possess multiple functionalities as well as flexibility in different physical arrangements. In the SA-based active sensing approach, one actuating SA generates excitation waves to other, nearby sensing SAs. During this process, the damage status of the propagating medium in the wave path between SAs can be analyzed (Song *et al*. 2008). This method has been widely adopted in civil structure health monitoring (Xu *et al*. 2013, Zhang and Su 2017).

When the medium between the actuator and the sensor is undamaged, stress waves can propagate mostly unimpeded. However, when a crack is present in the medium, stress waves will reflect and diffract at the interface of the crack. Thus, the energy of the received signal will be attenuated. Fig. 3 shows the numerical simulation of stress wave propagation under different degree of cracking (no crack, 20mm long crack, and 50mm long crack) in a 2D concrete block. Fig. 3 demonstrates several underlying principles of active sensing: SA generated stress waves can propagate in concrete and be

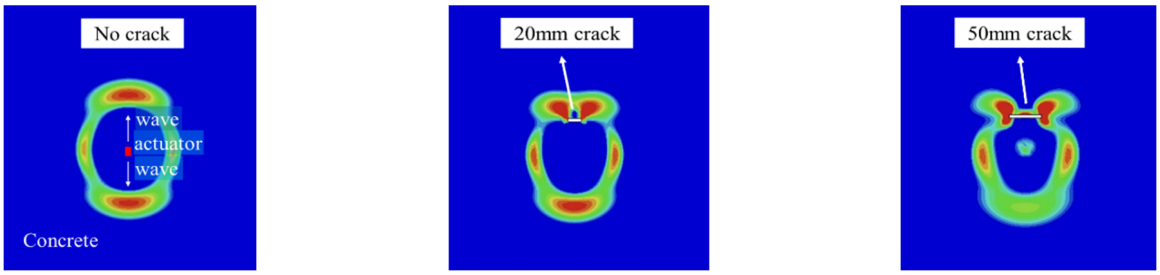

(a) With no crack (b) With 20 mm crack (c) With 50 mm crack

Fig. 3 Simulation of a stress wave propagating in a 2D concrete block

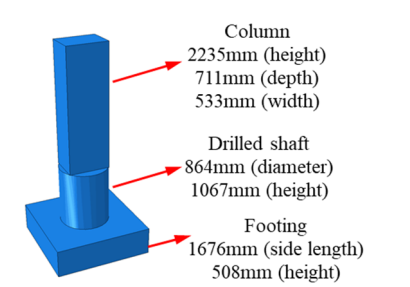

(a) Dimensions of the specimen model

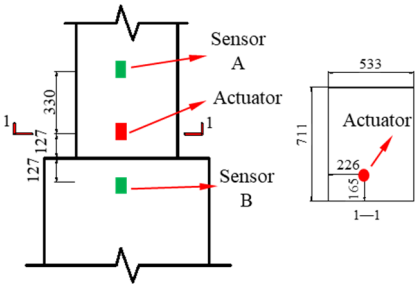

(b) Location of the distributed SAs (mm)

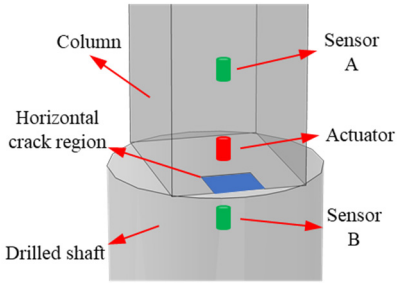

(c) Horizontal crack model

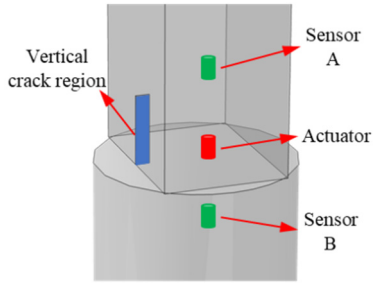

(d) Vertical crack model

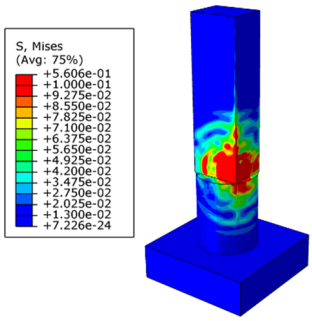

(e) Stress wave propagation in the horizontal crack model

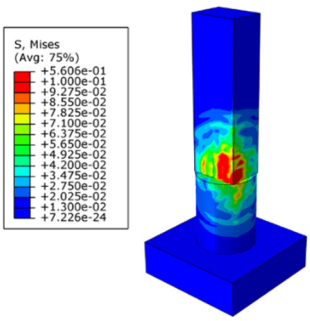

(f) Stress wave propagation in the vertical crack model

Fig. 4 Numerical specimen model description

sensed; the energy of the stress wave will attenuate due to reflection and diffraction at crack interfaces; the larger the size of the crack, the weaker the signal received by the sensor. Through the above principles, the active sensing approach can identify structural damage and evaluate the degree of damage.

3. Numerical study

In order to verify the effectiveness of the active sensing approach in the detection of damage in the variable cross section region of a column-drilled shaft assembly, a numerical simulation was conducted using the commercial software Abaqus. The column-drilled shaft assembly consists of a cuboid column, a cylindrical drilled shaft, and a square footing, as shown in Fig. 4(a). The dimensions of the column are 2235 mm in height, 711 mm in depth, and 533 mm in width. The diameter and height of the cylindrical drilled shaft are 864 mm and 1067 mm, respectively. The square footing is 508 mm in height and 1676 mm in side length. The concrete is assumed to be

Table 1 Material properties of the concrete

Density	Poisson's ratio	Elastic modulus
2500 kg/m³	0.2	30000 N/mm²

Table 2 Crack dimensions in four cases

	Horizontal crack			Vertical crack		
	Width (mm)	Length (mm)	Depth (mm)	Width (mm)	Length (mm)	Depth (mm)
No crack	—	—	—	—	—	—
Case 1	2	200	200	2	100	20
Case 2	2	300	300	2	200	40
Case 3	2	400	400	2	300	60

isotropic, and its material properties are listed in Table 1. Fig. 4(b) shows the arrangement of the three SAs, which are at the same locations as the experiment (Section 3). To maintain both computational stability and efficiency, the time increment Δt and the element type are set to 1E-7 s and three-dimensional, 8-node linear brick, reduced integration solid element (C3D8R), respectively.

To simulate damage cases at variable cross-section region of the column-drilled shaft assembly, a horizontal crack and a vertical crack were established in two simulation models, respectively. Figs. 4(c) and 4(d) show crack pattern and crack location at the variable cross-section region. The crack pattern adopted in simulation model is rectangular. Since the simulation analysis is to verify the effectiveness of the active sensing approach in the detection of damage in the variable cross-section region of a column-drilled shaft assembly, crack pattern is simplified by rectangular shape. Both horizontal crack model and vertical crack model have four cases corresponding to different levels of crack damage. The specific crack dimensions at different cases are listed in Table 2. In each case, the middle SA generates a three-cycle 50 kHz sinusoidal stress wave signal and the other two SAs receive signals. Figs. 4(e) and 4(f) show the snapshots of the stress wave propagation in horizontal crack model and vertical crack model, respectively.

Specifically, Signal A refers to the signal measured by Sensor A, and Signal B refers to the signal measured by Sensor B in the drilled shaft assembly. In order to eliminate the interference from reflected waves, the amplitude of the first peak of the acquired signals is selected and normalized for comparison.

Figs. 5(a) and 5(b) compare the received signals from four cases in the horizontal crack model. Since the location of the horizontal crack is not on the propagation path of Signal A, the expansion of the horizontal crack did little change to the amplitude of the first peak of Signal A. After normalization against the healthy base line (i.e., no crack), the amplitudes of the first peak in Signal A are 93%, 89%, and 80% for cases 1-3 respectively. Since the horizontal crack is in the propagation path of Signal B, the amplitude of Signal B changes significantly as the horizontal crack severity progressed over the four cases. As the horizontal crack expanded, the amplitude of the first peak in cases 1-3 decreased dramatically to 58%, 2%, 0% the case without a horizontal crack. This demonstrates that the SA-based active sensing approach is very sensitive to horizontal crack damage. Figs. 5(c) and 5(d) compare the signals from four cases in the vertical crack model. With the development of the investigated vertical crack, the amplitudes of the first peak of Signal A and Signal B decrease. Although the attenuation ratio for vertical crack condition is much

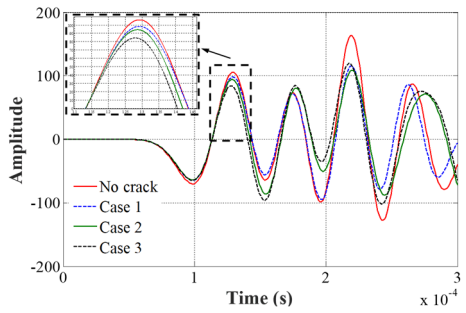

(a) Signal A collected from horizontal crack model

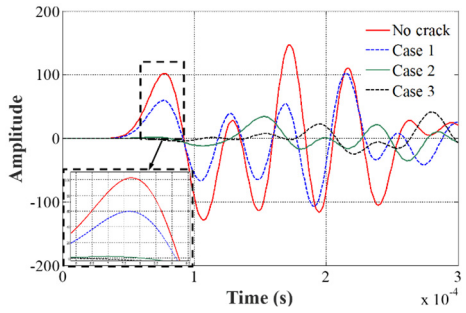

(b) Signal B collected from horizontal crack model

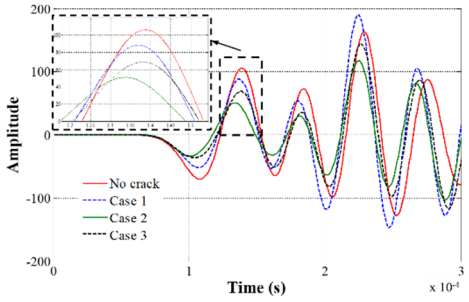

(c) Signal A collected from vertical crack model

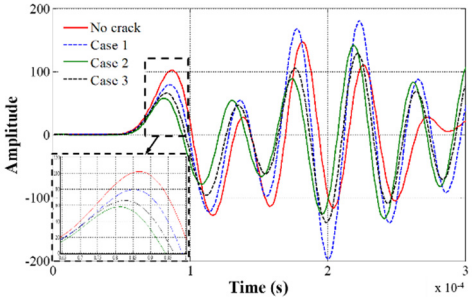

(d) Signal B collected from vertical crack model

Fig. 5 Numerical results of sensing signal from four simulation cases

smaller than that for horizontal crack condition, the proposed method is still effective to quantify the structural damage in case of vertical cracks.

The simulation results show that both horizontal and vertical cracks attenuate the stress wave energy between SA actuator and sensor. In this research, the SA-based active sensing approach offers a solution to comprehensively evaluate the damage condition of drilled shaft assembly with horizontal cracks and vertical cracks. The numerical studies in this section prove the feasibility of using distributed SAs to monitor multi-directional cracks in variable cross-section region of column-drilled shaft assembly.

4. Experimental setup and procedure

4.1 Details of the column-drilled shaft assembly

A test specimen consisting of a column-drilled shaft assembly was designed for the experiment. The dimensions of the assembly are shown in Fig. 4(a). Fig. 6 illustrates the reinforcement configuration of the specimen. The column and the drilled shaft have vertical reinforcements respectively comprising of 20 and 30 #5 bars. At places where the cross section varies, 20 #5 dowel bars are deployed to strengthen the connection. The length of the drilled shaft and the column are both 749 mm.

The compressive strength of the specimen was measured from an unconfined compression test using 101.6 mm (diameter) × 203.2 mm (height) cylinder specimens one day prior to the loading test. Table 3 lists the material parameters of the specimens, including the yield and tensile strengths for the different bars. The deformed steel bars follow ASTM A615 standards, which dictate a material strength of Grade 60.

Two groups of SAs were installed on the tensioned side of the column-drilled shaft (Fig. 6). In each group, three SAs were lined vertically, with the middle one serving as the actuator, and the other two serving as sensors. The SA actuator was situated above the interface between the column and the drilled shaft, and two SA sensors were embedded in the column and the drilled shaft, respectively.

When the variable cross-section region cracked, the stress wave energy will decrease. Therefore, the damage information in the variable cross-section region can be characterized by the energy attenuation in the monitored signals. In this way, the location and sequence of cracks can be monitored and compared with the development of cracks observed and manually recorded during the experiment.

4.2 Installation and location of SAs

During the process of assembling the reinforcement, two groups of SAs were installed on the dowel bars. To monitor the initiation and development of cracks, SAs were placed on the tension side (north side) of the specimen, as shown in Fig. 7(a). The tension side possessed 6 dowel bars in total, and two groups of SAs (three in each group) were vertically arranged on the first and the third dowel bars respectively, as shown in Fig. 7(b). In each group of SAs, the middle one (SA2 and SA4) transmitted stress waves, while the other two received signals.

4.3 Experimental setup

The setup for applying a uniform bending moment on the column-drilled shaft assembly is shown in Fig. 8(a). The base of the drilled shaft was tension-anchored to the strong floor using 16 high strength threaded rods (31.75 mm diameter). A steel box beam was connected to the top of the column using embedded anchors at the top of the column and through threaded rods on the side of the column. The

Table 3 Material parameters of concrete and deformed steel bars

		Unconfined compressive strength, N/mm²	
Concrete		Column	Drilled shaft
		45.8	50.6
Deformed steel bars	Bar size	Yield stress, N/mm²	Tensile strength, N/mm²
	#3	430.9	663.5
	#5	452.1	721.6

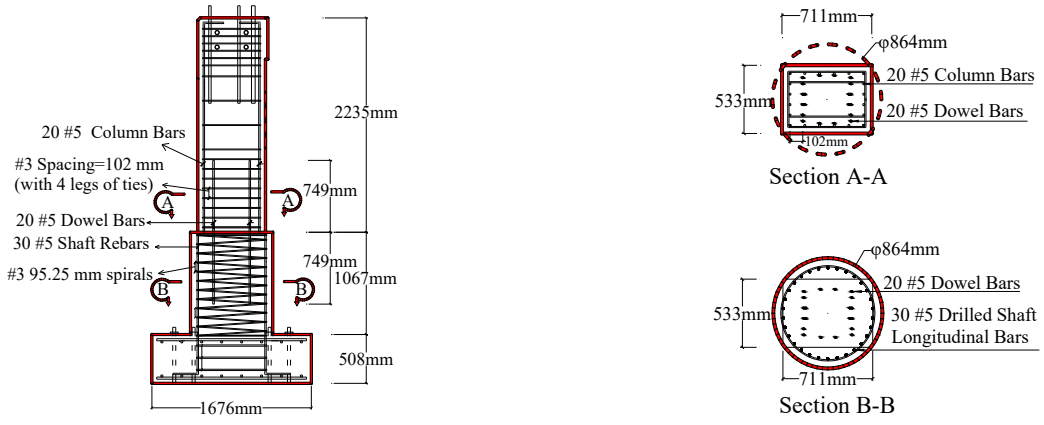

(a) Vertical section (b) Cross section

Fig. 6 Reinforcements in the specimen

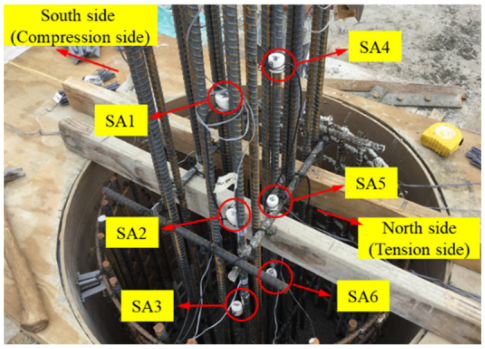

(a) Installation of SAs on dowel bars

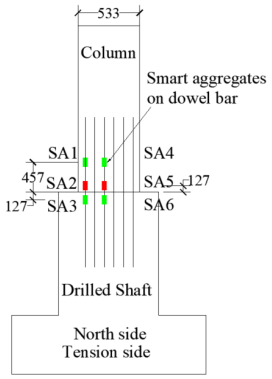

(b) Location of SAs (mm)

Fig. 7 Fabrication of the test specimen installed with SAs

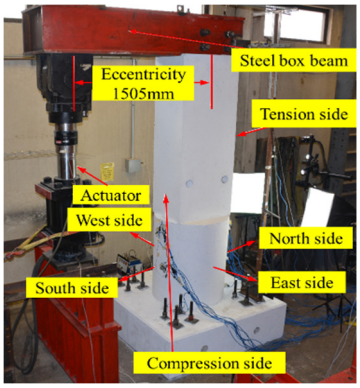

(a) Laboratory test setup

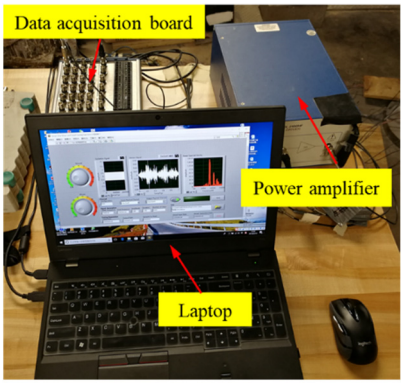

(b) Instrumental setup

Fig. 8 Experimental setup

load was implemented on the steel box beam, and was applied with an eccentricity of 1505 mm from the centerline of the column to create uniform bending moment in the column-drilled shaft assembly. A 980 kN (in tension) servo-controlled hydraulic actuator reacted against a steel reaction beam that was bolted to the strong floor to the generate the vertical, downward load. Fig. 8(b) shows the data acquisition (DAQ) system, which included a DAQ board (NI USB X Series 6361, National Instruments, Austin, TX, USA), a power amplifier (TREK Model 2100HF, Terk Inc, Lockport, NY, USA), and a laptop as monitoring terminal in the experiment.

4.4 Test procedures

The test specimen was monotonically loaded to 296.9 kN, and the whole loading process lasted about 2 hours. During loading, four signals (received by SA1, SA3, SA4, SA6) were collected every five minutes. At each measurement, actuators (SA2/SA5) generated a swept sine wave (200 Hz to 200 kHz at 10 V amplitude over 1 s). Signals received by sensors were recorded by the DAQ system.

5. Experimental results

5.1 Structural behavior

Fig. 9 shows the load vs. time curve of the specimen in the experiment. During the loading process, cracks on the surface of the specimen were recorded in detail and numbered in the order of appearance. The appearance of cracks was marked with black dots as shown in Fig. 9. A total of six main cracks (i.e., cracks 1-6) appeared, as shown in Fig. 10. All the main cracks formed on tension side of the

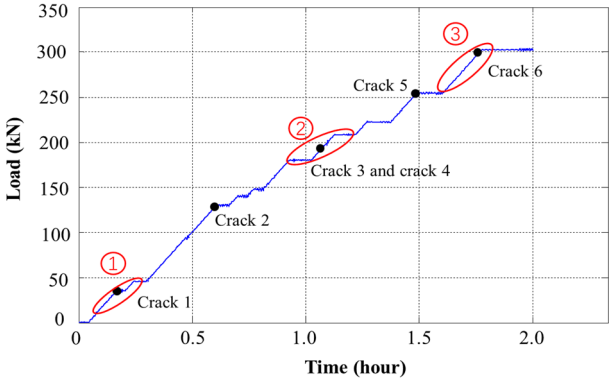

Fig. 9 The load vs. time curve of the specimen

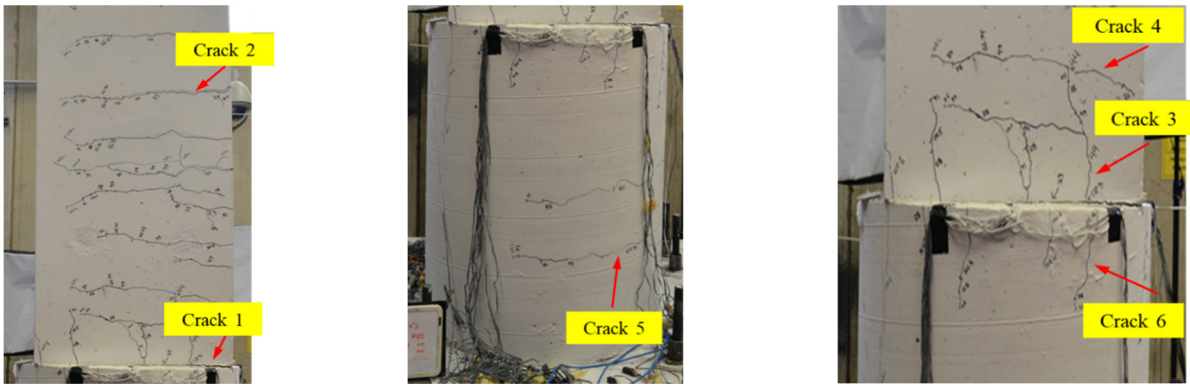

(a) Cracks on the column (b) Cracks on the drilled shaft (c) Cracks near the interface of column-drilled shaft

Fig. 10 Surface of the column-drilled shaft assembly after testing

concrete. The observation records indicated that horizontal cracks appeared on the tension side and developed towards the compression side. Four of the six cracks (cracks 1, 2, 4, and 5) are horizontal cracks, and two (crack 3, crack 6) are vertical cracks. Cracks 1-4 appeared on the surface of the column, and cracks 5-6 appeared on the surface of the drilled shaft. Stage ① to ③ refer to the crack initiation, crack development, and end of the test, respectively. This demonstrated that damage to the variable cross-section first occurred at the bottom end of the column, and then appeared at the top of the drilled shaft.

5.2 Damage index and wavelet packet analysis

The damage index derived from the wavelet packet decomposition is a commonly used method for signal processing in structural health monitoring (Wang *et al.* 2019). In this paper, a damage index was established as follows. Firstly, a signal X can be decomposed into 2^n signal sets $\{X_1, X_2, \cdots, X_j, \cdots, X_{2^n}\}$ through n-level wavelet packet decomposition, where X_j is given in Eq. (1). The signal energy is the sum of the squares of each set of signals (Eq. (2)). The energy vector E_i at i^{th} measurement is specified in Eq. (3).

$$X_j = [x_{j,1}, x_{j,2}, \cdots, x_{j,m}] \tag{1}$$

$$E_{i,j} = \|X_j\|_2^2 = x_{j,1}^2 + x_{j,2}^2 + \cdots + x_{j,m}^2 \tag{2}$$

$$E_i = [E_{i,1}, E_{i,2}, \cdots, E_{i,2^n}] \tag{3}$$

where j is the frequency band ($j = 1, \cdots, 2^n$), m is the data length, and i is the measurement point when the sensor signal is collected.

The energy vector of the signal X_0 in the initial healthy state is defined as $E_0 = [E_{0,1}, E_{0,2}, \cdots, E_{0,2^n}]$. The energy vector of signal X_i at measurement i is defined as $E_i = [E_{i,1}, E_{i,2}, \cdots, E_{i,2^n}]$. The damage index ($DI$) at measurement i can be established from Eq. (4) (Song *et al.* 2008).

$$DI = \sqrt{\frac{\sum_{j=1}^{2^n}(E_{i,j} - E_{0,j})^2}{\sum_{j=1}^{2^n} E_{0,j}^2}} \tag{4}$$

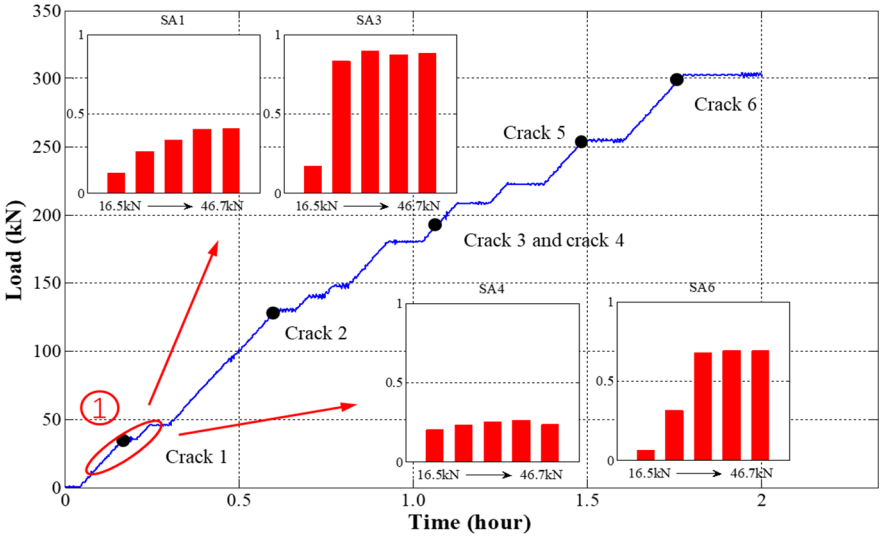

Fig. 11 Damage indices in stage ①

The damage index represents the energy loss ratio of the signal collected at measurement *i* to the healthy status signal, and ranges from zero to one. At the initial time, the structure is healthy with no damage, and the index value is zero. When damage occurs, the transmitted energy of the stress wave decreases and the damage index value increases correspondingly. In the extreme case, the structural damage is so severe that the stress wave signal cannot be received, and the damage index value approaches to one.

5.3 Monitoring results

It should be specified that the locations of crack 2 and crack 5 are outside the monitoring range of the SAs, and the corresponding damage index results are not presented in this paper. In order to understand out the correlation between damage indices and cracks, three stages (marked by red ovals in Fig. 9) of damage indices related to crack development are analyzed.

Stage ①: At a load of 35.6 kN, crack 1 occurred at the interface between the column and the drilled shaft, demonstrating that the interface was the weakest position of the specimen. The damage indices for stage ①, (i.e., loading from 16.5 kN to 46.7 kN) is shown in Fig. 11. Since crack 1 appeared below the actuators (SA2 and SA5), the changes in the *DI* of SA3 and *DI* of SA6 were particularly large in stage ①. The *DI* of SA3 increased from 0.17 to 0.9, and the *DI* of SA6 increased from 0.06 to 0.69. The *DI* of SA3 was larger because crack 1 was closer to SA2. It is notable that the *DI* of SA3 reached a very high value (0.9), thus precluding further significant increases in subsequent experiments. The *DI* of SA1 and *DI* of SA4 both increased slightly, indicating that the concrete in the column also suffered damage when crack 1 occurred. When loading to 129 kN, crack 2 appeared at the top on the column near the upper end of the dowel bars.

Fig. 12 shows the time domain signals corresponding to the damage indices in stage ①. No obvious changes can be observed in the SA1 signals (Fig. 12(a)) and SA4 signals (Fig. 12(c)). In contrast, the SA3 signals (Fig. 12(b)) and SA6 signals (Fig. 12(d)) experienced visible changes. When the load increased from 16.5 kN to 30 kN, the amplitude of SA3 signal decreased significantly, and the trend fits well with the damage indices. A similar phenomenon can also be observed in the behavior of the SA6 signals when the load increased from 30 kN to 35 kN. By comparing the time domain signals with the damage indices, the wavelet packet-based damage index can accurately describe the attenuation of the signal during the loading process. Furthermore, the damage index analysis is highly sensitive to signal changes and is more efficient than visually analyzing the time-domain signals.

Stage ②: When the load increased to195.7 kN, crack 3 and crack 4 appeared simultaneously near the bottom of the column. When the load increased from 181 kN to 209 kN (stage ②), the *DI* of SA1 increased from 0.8 to 0.97, the *DI* of SA4 increased from 0.67 to 0.91, and the *DI* of SA6 increased from 0.62 to 0.79. At 250.2 kN, crack 5 occurred at the bottom on the drilled shaft near the lower end of the dowel bars. Fig. 13 shows the damage indices in stage ②.

Stage ③: At 293.6 kN, crack 3 extended from the bottom of the column to the top of the drilled shaft and formed crack 6. In stage ③ (loading from 254 kN to 302.9 kN), except for the small increase of *DI* of SA6 (from 0.85 to 0.98), the other signal damage indices approached 1, and there were no significant changes, as shown in Fig. 14.

The monitoring results demonstrated that the wavelet packet based *DI* method can accurately monitor the internal damage in the variable cross-section region near the interface of the column and the drilled shaft. The results

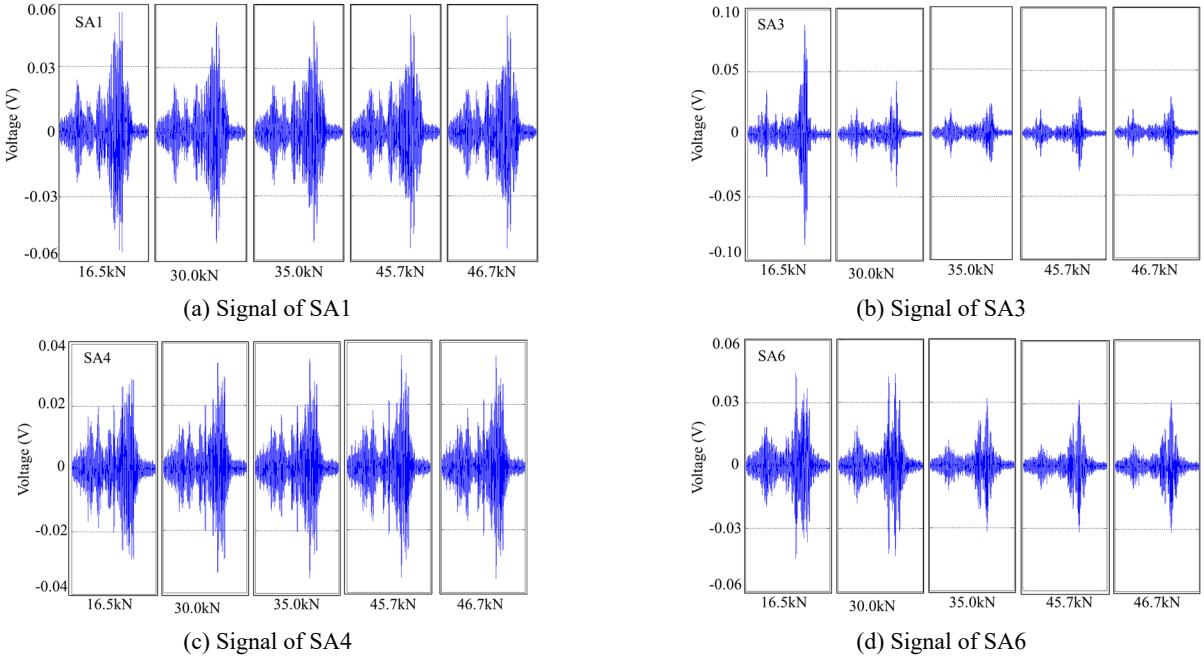

(a) Signal of SA1

(b) Signal of SA3

(c) Signal of SA4

(d) Signal of SA6

Fig. 12 Time domain signal comparison in stage ①

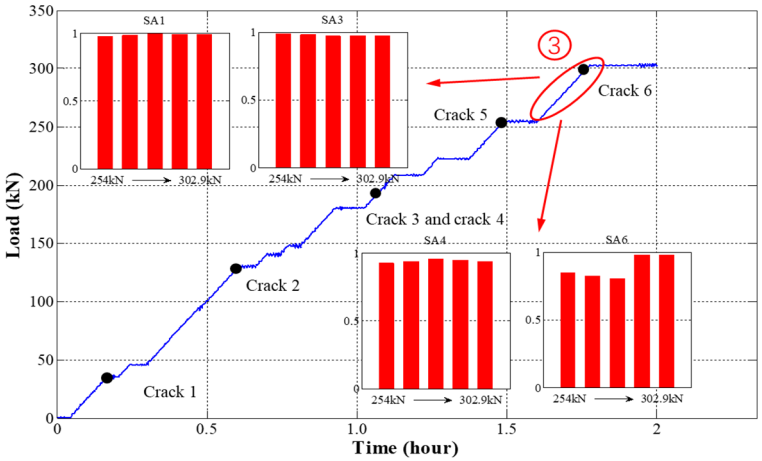

Fig. 14 Damage indices in stage ③

agree well with the crack development process observed in the experiment. It should be noted that the changes in damage indices precede the occurrence of surface cracks, demonstrating the effectiveness of proposed method for providing early warning of damage.

6. Discussions

In this research, SA-based technology was studied to monitor crack damage in a column-drilled shaft assembly. Though both numerical and experimental results prove the feasibility and validity of the proposed method, there are several drawbacks that limit the current SA-based technology in the field application. Firstly, SAs have to be installed at the pre-determined location during concrete casting, which means the proposed method can hardly be used to monitor existing structures. Secondly, the area or volume covered by this monitoring method is limited by how the SAs are distributed in the structure. If the crack damage does not occur between the deployed SA pair, those cracks cannot be identified. Thirdly, SAs used in this research only generate and receive one-dimensional wave, therefore the orientation of SAs should be carefully designed to fulfil the detection purpose. Fourthly, due to the limitation of existing technology, the only possible way to compare and confirm the validity of the proposed method is checking the surface cracks from the test specimens. Though the results from checking surface cracks cannot precisely reflect the real crack condition inside the concrete columns, the authors have delivered their best to collect all the experimental observation findings to prove the validity and accuracy of the proposed method. In the authors' future work, the current SA design and its installation procedure will be improved to enhance the field application possibility.

7. Conclusions

In this study, SAs are installed in the variable cross-section region of a column-drilled shaft assembly to provide real time monitoring of the damage severity during loading. The wavelet packet-based *DI* coupled with the active sensing approach were adopted to generate and analyze signals to quantify the degree of damage at different parts of a specimen. The comparison between the monitoring results from a monotonic loading test and the experimentally observed crack records shows that the changes in the damage index precedes the occurrence of visible cracks. The behavior of the *DI* over the course of the test corroborates with the crack evolution, thereby demonstrating the accuracy of the presented monitoring methods. The results also demonstrate that SA-based technologies and evaluation methods are suitable for generating early warnings for potential damage in reinforced concrete structures.

Acknowledgments

The research described in this paper was supported by the Texas Department of Transportation (Award number 0-6914), U.S., National Natural Science Foundation of China (Grant number 51978507; 52020105005), Science and Technology Commission of Shanghai Municipality (Grant number 19DZ1201200).

References

Banjara, N.K., Sasmal, S. and Srinivas, V. (2019), "Damage progression study in fibre reinforced concrete using acoustic emission technique", *Smart Struct. Syst., Int. J.*, **23**(2), 173-184. https://doi.org/10.12989/sss.2019.23.2.173

Berry, M.P., Lehman, D.E. and Lowes, L.N. (2008), "Lumped-plasticity models for performance simulation of bridge columns", *ACI Struct. J.*, **105**(3), 270. https://doi.org/10.14359/19786

Feng, Q., Kong, Q., Huo, L. and Song, G. (2015), "Crack detection and leakage monitoring on reinforced concrete pipe", *Smart Mater. Struct.*, **24**(11), 115020. https://doi.org/10.1088/0964-1726/24/11/115020

Feng, Q., Kong, Q. and Song, G. (2016), "Damage detection of concrete piles subject to typical damage types based on stress wave measurement using embedded smart aggregates

transducers", *Measurement*, **88**, 345-352. https://doi.org/10.1016/j.measurement.2016.01.042

Feng, Q., Kong, Q., Jiang, J., Liang, Y. and Song, G. (2017), "Detection of interfacial debonding in a rubber–steel-layered structure using active sensing enabled by embedded piezoceramic transducers", *Sensors*, **17**(9), 2001. https://doi.org/10.3390/s17092001

Feng, Q., Tang, M. and Ou, J. (2020), "Monolithic multicore fiber based multi-parameter measurement based on spatial-division-multiplex sensing mechanisms", *Measurement*, **151**, 107128. https://doi.org/10.1016/j.measurement.2019.107128

Gu, H., Moslehy, Y., Sanders, D., Song, G. and Mo, Y.L. (2010), "Multi-functional smart aggregate-based structural health monitoring of circular reinforced concrete columns subjected to seismic excitations", *Smart Mater. Struct.*, **19**(6), 065026. https://doi.org/10.1088/0964-1726/19/6/065026

Hou, S., Zhang, H.B. and Ou, J.P. (2012), "A PZT-based smart aggregate for compressive seismic stress monitoring", *Smart Mater. Struct.*, **21**(10), 105035. https://doi.org/10.1088/0964-1726/21/10/105035

Hou, S., Zhang, H.B. and Ou, J.P. (2013), "A PZT-based smart aggregate for seismic shear stress monitoring", *Smart Mater. Struct.*, **22**(6), 065012. https://doi.org/10.1088/0964-1726/22/6/065012

Howser, R., Moslehy, Y., Gu, H., Dhonde, H., Mo, Y.L., Ayoub, A. and Song, G. (2011), "Smart-aggregate-based damage detection of fiber-reinforced-polymer-strengthened columns under reversed cyclic loading", *Smart Mater. Struct.*, **20**(7), 075014. https://doi.org/10.1088/0964-1726/20/7/075014

Huo, L., Cheng, H., Kong, Q. and Chen, X. (2019), "Bond-slip monitoring of concrete structures using smart sensors—A review", *Sensors*, **19**(5), 1231. https://doi.org/10.3390/s19051231

Huynh, T.C., Lee, K.S. and Kim, J.T. (2015), "Local dynamic characteristics of PZT impedance interface on tendon anchorage under prestress force variation", *Smart Struct. Syst., Int. J.*, **15**(2), 375-393. http://doi.org/10.12989/sss.2015.15.2.375

Jiang, J., Hei, C., Feng, Q. and Jiang, J. (2019), "Monitoring of epoxy-grouted bonding strength development between an anchored steel bar and concrete using PZT-enabled active sensing", *Sensors*, **19**(9), 2096. https://doi.org/10.3390/s19092096

Jiang, J., Jiang, J., Deng, X. and Deng, Z. (2020), "Detecting debonding between steel beam and reinforcing CFRP plate using active sensing with removable PZT-Based transducers", *Sensors*, **20**(1), 41. https://doi.org/10.3390/s20010041

Karayannis, C.G., Voutetaki, M.E., Chalioris, C.E., Providakis, C.P. and Angeli, G.M. (2015), "Detection of flexural damage stages for RC beams using piezoelectric sensors (PZT)", *Smart Struct. Syst., Int. J.*, **15**(4), 997-1018. https://doi.org/10.12989/sss.2015.15.4.997

Kong, Q., Hou, S., Ji, Q., Mo, Y.L. and Song, G. (2013), "Very early age concrete hydration characterization monitoring using piezoceramic based smart aggregates", *Smart Mater. Struct.*, **22**(8), 085025. https://doi.org/10.1088/0964-1726/22/8/085025

Kong, Q., Robert, R.H., Silva, P. and Mo, Y.L. (2016), "Cyclic crack monitoring of a reinforced concrete column under simulated pseudo-dynamic loading using piezoceramic-based smart aggregates", *Applied Sci.*, **6**(11), 341. https://doi.org/10.3390/app6110341

Kong, Q., Chen, H., Mo, Y.L. and Song, G. (2017a), "Real-time monitoring of water content in sandy soil using shear mode piezoceramic transducers and active sensing—A feasibility study". *Sensors*, **17**(10), 2395. https://doi.org/10.3390/s17102395

Kong, Q., Fan, S., Bai, X., Mo, Y.L. and Song, G. (2017b), "A novel embeddable spherical smart aggregate for structural health monitoring: Part I. Fabrication and electrical characterization", *Smart Mater. Struct.*, **26**(9), 095050. https://doi.org/10.1088/1361-665x/aa80bc

Kong, Q., Fan, S., Mo, Y.L. and Song, G. (2017c), "A novel embeddable spherical smart aggregate for structural health monitoring: Part II. Numerical and experimental verifications", *Smart Mater. Struct.*, **26**(9), 095051. https://doi.org/10.1088/1361-665x/aa80ef

Kuang, K.S.C. and Cantwell, W.J. (2003), "Use of conventional optical fibers and fiber Bragg gratings for damage detection in advanced composite structures: a review", *Appl. Mech. Rev.*, **56**(5), 493-513. https://doi.org/10.1115/1.1582883

Li, H.N., Li, D.S. and Song, G.B. (2004), "Recent applications of fiber optic sensors to health monitoring in civil engineering", *Eng. Struct.*, **26**(11), 1647-1657. https://doi.org/10.1016/j.engstruct.2004.05.018

Li, W., Kong, Q., Ho, S.C.M., Mo, Y.L. and Song, G. (2016), "Feasibility study of using smart aggregates as embedded acoustic emission sensors for health monitoring of concrete structures", *Smart Mater. Struct.*, **25**(11), 115031. https://doi.org/10.1088/0964-1726/25/11/115031

Liang, Y., Li, D., Parvasi, S.M., Kong, Q. and Song, G. (2016), "Bond-slip detection of concrete-encased composite structure using electro-mechanical impedance technique", *Smart Mater. Struct.*, **25**(9), 095003. https://doi.org/10.1088/0964-1726/25/9/095003

Liu, T., Huang, Y., Zou, D., Teng, J. and Li, B. (2013), "Exploratory study on water seepage monitoring of concrete structures using piezoceramic based smart aggregates", *Smart Mater. Struct*, **22**(6), 065002. https://doi.org/10.1088/0964-1726/22/6/065002

Markovic, N., Nestorovic, T. and Stojic, D. (2015), "Numerical modeling of damage detection in concrete beams using piezoelectric patches", *Mech. Res. Commun.*, **64**, 15-22. https://doi.org/10.1016/j.mechrescom.2014.12.007

Motaref, S., Saiidi, M.S. and Sanders, D. (2014), "Shake table studies of energy-dissipating segmental bridge columns", *J. Bridge Eng.*, **19**(2), 186-199. https://doi.org/10.1061/(ASCE)BE.1943-5592.0000518

Nguyen, K.D., Ho, D.D. and Kim, J.T. (2013), "Damage detection in beam-type structures via PZT's dual piezoelectric responses", *Smart Struct. Syst., Int. J.*, **11**(2), 217-240. https://doi.org/10.12989/sss.2013.11.2.217

Pan, X., Liang, D. and Li, D. (2006), "Optical fiber sensor layer embedded in smart composite material and structure", *Smart Mater. Struct.*, **15**(5), 1231. https://doi.org/10.1088/0964-1726/15/5/010

Qin, F., Kong, Q., Li, M., Mo, Y.L., Song, G. and Fan, F. (2015), "Bond slip detection of steel plate and concrete beams using smart aggregates", *Smart Mater. Struct.*, **24**(11), 115039. https://doi.org/10.1088/0964-1726/24/11/115039

Quant, M., Elizalde, H., Flores, A., Ramírez, R., Orta, P. and Song, G. (2009), "A comprehensive model for piezoceramic actuators: modelling, validation and application", *Smart Mater. Struct.*, **18**(12), 125011. https://doi.org/10.1088/0964-1726/18/12/125011

Song, G., Gu, H. and Mo, Y.L. (2008), "Smart aggregates: multi-functional sensors for concrete structures—a tutorial and a review", *Smart Mater. Struct.*, **17**(3), 033001. https://doi.org/10.1088/0964-1726/17/3/033001

Wang, F., Huo, L. and Song, G. (2017), "A piezoelectric active sensing method for quantitative monitoring of bolt loosening using energy dissipation caused by tangential damping based on the fractal contact theory", *Smart Mater. Struct.*, **27**(1), 015023. https://doi.org/10.1088/1361-665x/aa9a65

Wang, Z., Wei, L. and Cao, M. (2019), "Damage Quantification with Embedded Piezoelectric Aggregates Based on Wavelet

Packet Energy Analysis", *Sensors*, **19**(2), 425. https://doi.org/10.3390/s19020425

Wang, F., Chen, Z. and Song, G. (2020), "Monitoring of multi-bolt connection looseness using entropy-based active sensing and genetic algorithm-based least square support vector machine", *Mech. Syst. Signal Process.*, **136**, 106507. https://doi.org/10.1016/j.ymssp.2019.106507

Xu, B., Zhang, T., Song, G. and Gu, H. (2013), "Active interface debonding detection of a concrete-filled steel tube with piezoelectric technologies using wavelet packet analysis", *Mech. Syst. Signal Process.*, **36**(1), 7-17. https://doi.org/10.1016/j.ymssp.2011.07.029

Yan, S., Sun, W., Song, G., Gu, H., Huo, L.S., Liu, B. and Zhang, Y.G. (2009), "Health monitoring of reinforced concrete shear walls using smart aggregates", *Smart Mater. Struct.*, **18**(4), 047001. https://doi.org/10.1088/0964-1726/18/4/047001

Yao, P., Kong, Q., Xu, K., Jiang, T., Huo, L.S. and Song, G. (2015), "Structural health monitoring of multi-spot welded joints using a lead zirconate titanate based active sensing approach", *Smart Mater. Struct.*, **25**(1), 015031. https://doi.org/10.1088/0964-1726/25/1/015031

Zeng, L., Parvasi, S.M., Kong, Q., Huo, L., Li, M. and Song, G. (2015), "Bond slip detection of concrete-encased composite structure using shear wave based active sensing approach", *Smart Mater. Struct.*, **24**(12), 125026. https://doi.org/10.1088/0964-1726/24/12/125026

Zhang, N. and Su, H. (2017), "Application assessments of concrete piezoelectric smart module in civil engineering", *Smart Struct. Syst., Int. J.*, **19**(5), 499-512. https://doi.org/10.12989/sss.2017.19.5.499

Zhang, J., Li, Y., Huang, Y., Jiang, J. and Ho, S.C.M. (2018a), "A feasibility study on timber moisture monitoring using piezoceramic transducer-enabled active sensing", *Sensors*, **18**(9), 3100. https://doi.org/10.3390/s18093100

Zhang, J., Huang, Y. and Zheng, Y. (2018b), "A feasibility study on timber damage detection using piezoceramic-transducer-enabled active sensing", *Sensors*, **18**(5), 1563. https://doi.org/10.3390/s18051563

Zou, D., Du, C., Liu, T. and Li, W. (2019), "Effects of temperature on the performance of the piezoelectric-based smart aggregates active monitoring method for concrete structures", *Smart Mater. Struct.*, **28**(3), 035016. https://doi.org/10.1088/1361-665x/aafe15.

BS